ARMY RESEARCH LABORATORY

Implications of Gun Propellant Bed Rheology

Paul J. Conroy
Douglas E. Kooker

ARL-TR-80 February 1993

NOTICES

Destroy this report when it is no longer needed. DO NOT return it to the originator.

Additional copies of this report may be obtained from the National Technical Information Service, U.S. Department of Commerce, 5285 Port Royal Road, Springfield, VA 22161.

The findings of this report are not to be construed as an official Department of the Army position, unless so designated by other authorized documents.

The use of trade names or manufacturers' names in this report does not constitute indorsement of any commercial product.

REPORT DOCUMENTATION PAGE

Form Approved
OMB No. 0704-0188

1. AGENCY USE ONLY *(Leave blank)*	2. REPORT DATE	3. REPORT TYPE AND DATES COVERED
	February 1993	Final, Dec 90–Dec 91

4. TITLE AND SUBTITLE

Implications of Gun Propellant Bed Rheology

5. FUNDING NUMBERS

PR: 1L161102AH43

6. AUTHOR(S)

Paul J. Conroy and Douglas E. Kooker

7. PERFORMING ORGANIZATION NAME(S) AND ADDRESS(ES)

8. PERFORMING ORGANIZATION REPORT NUMBER

9. SPONSORING / MONITORING AGENCY NAME(S) AND ADDRESS(ES)

U.S. Army Research Laboratory
ATTN: AMSRL-OP-CI-B (Tech Lib)
Aberdeen Proving Ground, MD 21005-5066

10. SPONSORING / MONITORING AGENCY REPORT NUMBER

ARL-TR-80

11. SUPPLEMENTARY NOTES

12a. DISTRIBUTION / AVAILABILITY STATEMENT

Approved for public release; distribution is unlimited.

12b. DISTRIBUTION CODE

13. ABSTRACT *(Maximum 200 words)*

Simulation of the interior ballistic cycle for certain gun systems can sometimes predict the growth of pressure waves to potentially dangerous amplitudes. Such predictions involve the propagation of large amplitude stress waves through a compressed aggregate of propellant grains. The fidelity of the simulation will depend upon the accuracy of the constitutive behavior assigned to the propellant bed. This report examines the current formulation in Gough's NOVA-series codes, and then explores the implications on effective wave propagation speed for two different materials: a brittle crystalline material (HMX) and a double-base ball propellant. The results indicate the potential importance of solid-phase compressibility at stress levels above 100 MPa.

14. SUBJECT TERMS	15. NUMBER OF PAGES
interior ballistics, pressure waves; compressibility; wave propagation; rheology	33
	16. PRICE CODE

17. SECURITY CLASSIFICATION OF REPORT	18. SECURITY CLASSIFICATION OF THIS PAGE	19. SECURITY CLASSIFICATION OF ABSTRACT	20. LIMITATION OF ABSTRACT
UNCLASSIFIED	UNCLASSIFIED	UNCLASSIFIED	UL

INTENTIONALLY LEFT BLANK.

TABLE OF CONTENTS

INTENTIONALLY LEFT BLANK.

LIST OF FIGURES

INTENTIONALLY LEFT BLANK.

1. INTRODUCTION

During the design phase of any new gun system, it is important to evaluate the influence of various possible components and geometric configurations. In certain scenarios, simulation of the interior ballistic cycle will predict the growth of pressure waves to amplitudes which would threaten the integrity of the system. It is imperative to ensure the accuracy of these model predictions. Current interior ballistic simulations with Gough's XNOVAKTC code (Gough 1990) (hereafter called "XKTC") can, for example, predict propellant bed compression events where the value of the axial component of mixture stress exceeds 100 MPa. At the present time, there are no experimental data on mechanical behavior of a compacted bed of gun propellant grains at these stress levels, and hence *no way to validate the model predictions*. However, these data should eventually be available from a current Navy program (NSWC/ White Oak Labs) which involves compression of full scale (127mm diameter) granular propellant beds.

The present study is an effort to upgrade the description of mechanical properties assigned to the compacted propellant bed in the interior ballistic simulation. This report will attempt a brief review of the formulation currently used in the XKTC code (Gough 1990) and then discuss some alternative formulations which might be used to represent experimental data. Although an incompressible solid phase is a basic assumption in the XKTC code, the discussion here will address the implications of solid propellant compressibility on the predicted values of wave propagation speed in a compacted aggregate.

A number of experimental studies (Nicolaides, Wiegand, and Pinto 1980; Lieb and Rocchio 1982; Lieb 1989; Gazonas, Juhasz, and Ford 1991; Gazonas 1991; Lieb and Leadore 1991 & 1992) have produced valuable information concerning the mechanical properties of a single propellant grain. However, compression of an aggregate of propellant grains involves complex interactions at grain boundaries leading to sliding, deformation, and possible fracture (depending upon the type of material in question). Because of these interactions, it is not clear how the mechanical properties of a single grain can be used directly to construct the response of the compacted granular aggregate. The latter is required in interior ballistic models which employ an averaging technique to generate an elemental volume containing a binary mixture (i.e., that portion of the volume not occupied by the solid is assumed to be gas). An important consequence of this simplification is the necessity for a phenomenological sub-model to link porosity of the aggregate to its stress state. Clearly, the value of certain parameters used in the description of this stress state must be determined by matching the response of the sub-model to data from rheological experiments on compacted aggregates composed of a given solid material.

The grain-to-grain "resistance" forces associated with sliding, deformation, and fracture could conceivably introduce a strain-rate dependence into the constitutive behavior of the aggregate. At the present time, there is not a great deal of experimental data to guide a model (see review by Conroy 1991). Single grains of JA2, M30 and XM39 gun propellant which are subjected to compression in a Hopkinson Split Bar test (Lieb, 1991) show the presence of a strain-rate influence, as they do in the Servohydraulic tests (Gazonas 1991) at lower strain rates. However, combustion of these damaged grains in a closed bomb (Gazonas, Juhasz, and Ford 1991) indicates that the effective burning surface area is nearly independent of the strain-rate history of the sample. Apparently, the only modeling attempts to account for rate-dependence *within a two-phase mixture* have been limited to a "global" description (Baer and Nunziato 1986; Kooker 1990) which is difficult to calibrate. Currently, all two-phase interior ballistic models known to the authors have neglected rate dependence and assumed that changes in mixture density are accommodated by an instantaneous adjustment to the new stress state. This will be denoted here as the "equilibrium" stress state. Note that the values of stress and associated wave propagation speed predicted by the equilibrium stress state are lower bounds; if, in fact, rate dependence were present, changes in mixture density which occur at high-strain rate would lead to increased values. The validity of neglecting rate dependence must be reevaluated sometime in the future.

If the propellant bed will be subjected to a large amplitude stress field, another important consideration is the treatment of the solid-phase material itself. Compaction of a granular aggregate can involve changes in density of the solid grains as well as rearrangement and deformation of the grains. Quasi-static compaction experiments (e.g., Elban [1984]; Elban and Chiarito [1986], and Sandusky et al. [1988] are based on both inert and energetic materials of small grain diameter) typically monitor various stresses as a function of a changing mixture volume. To deduce the associated values of porosity (either void volume or solid volume fraction) requires a model of the mixture. If solid-phase density is assumed constant (incompressible), then porosity values are determined directly by the observed volume change. However, for many propellants of interest here, the incompressibility assumption can lead to a contradiction when analyzing compaction data at stress levels in the range of 100 MPa. When the solid-phase density is assumed constant, the experimental values of mixture volume will imply negative values of porosity (i.e., the mixture density has exceeded the theoretical maximum density [TMD] of the solid at atmospheric pressure [denoted here as TMD_o]). Since accounting for solid-phase compressibility eliminates this artificial result, the analysis below will examine the possible influence of propellant compressibility. Gough's (1974) mixture theory, which has been quite successful in simulating interior ballistics, does

assume an incompressible solid phase; this is a reasonable assumption as long as the magnitude of stress waves remains moderate.

When determining the constitutive behavior of an aggregate of propellant grains with a compaction experiment, the scale of the experiment (i.e., the ratio of the test-cell chamber diameter to the grain diameter) must be considered. A small-scale experiment involving full-size propellant grains will create a different porosity distribution and potentially a different interaction at the circumferential confining boundary. Since this could introduce unwanted distortions into the measured compaction response, it would be preferable to conduct the compaction experiment at full scale. Although full-scale propellant bed compaction data is meager or nonexistent at the current time, assume that such data will be available in the future. If the bed compaction experiment is conducted under quasi-static conditions (e.g., crosshead speeds of 0(10) cm/min), then for all practical purposes, it can be assumed that the results have not been influenced by strain rate. Thus the data can be used to construct or calibrate the rate-independent "equilibrium" stress state assigned to the propellant bed in the interior ballistic model (none of the models at the present time have a provision for a strain-rate effect). Since the NSWC/WO full-scale compaction experiment is to be conducted quasi-statically, a reasonable assumption is that the propellant bed remains isothermal. Furthermore, the pressure of the gas within the propellant bed can be assumed to remain at 1 atm since the tolerance between the rams and the inside of the cylindrical chamber will not prevent the escape of air trapped in the chamber.

2. MODEL DESCRIPTION OF THE PROPELLANT BED

To understand how the constitutive behavior of the compacted propellant bed is represented in the XKTC code (Gough 1980), consider a two-phase mixture composed of a compressible gas phase and a deformable but incompressible solid phase. Deformation of the mixture occurs in uniaxial strain only, along the axial direction, x. If we assume here that the mixture is confined within a channel of uniform cross-sectional area, then the mass balance for the solid phase can be written

$$\{\varepsilon_s\}_t + \{\varepsilon_s u_s\}_x = -\dot{m}/\rho_s \,, \tag{1}$$

where $\{\ \}_x$ denotes a partial derivative with respect to x, and $\{\ \}_t$ with respect to time. Although, in general, the solid-phase stress tensor will support deviator components, assume for this discussion that

deviator components are negligible; hence, the stress tensor can be represented with the spherical component (a pressure), P_s. The momentum balance for the solid phase can be written

$$\rho_s \varepsilon_s \frac{Du_s}{Dt_s} + \varepsilon_s \{P_s\}_x + (P_s - P_g)\{\varepsilon_s\}_x = f_d \ , \tag{2}$$

where D/Dt_s is the material derivative along the solid-phase streamline. Now let R_s represent the configuration stress, or that portion of P_s greater than P_g due to particle-particle contact when the granular solid phase is compacted into an aggregate. Gough (1980, 1974) refers to R_s as the "intrinsic average intergranular stress." With the further constraint that the force field at the interface between phases remains in equilibrium (i.e., $P_s = R_s + P_g$), the momentum balance becomes

$$\rho_s \varepsilon_s \frac{Du_s}{Dt_s} + \varepsilon_s \{P_g\}_x + \{\varepsilon_s R_s\}_x = f_d \ . \tag{3}$$

Let σ_s be Gough's "nonintrinsic average granular stress" defined as

$$\sigma_s \equiv \varepsilon_s R_s \ . \tag{4}$$

Now if R_s can be described by a strain-rate-independent function of solid volume fraction (or porosity), then $\sigma_s = \sigma_s(\varepsilon_s)$ and it follows that

$$\frac{d\sigma_s}{d\varepsilon_s} = \text{function}(\varepsilon_s) \equiv G(\varepsilon_s) \ , \tag{5}$$

and hence,

$$\{\sigma_s\}_x = G \cdot \{\varepsilon_s\}_x \ . \tag{6}$$

Thus the solid-phase momentum balance in Equation 3 can be written

$$\rho_s \varepsilon_s \frac{Du_s}{Dt_s} + \varepsilon_s \{P_g\}_x + G \cdot \{\varepsilon_s\}_x = f_d \ . \tag{7}$$

To visualize the role played by the function G, consider a compacted, granular mixture of incompressible solids under near-vacuum conditions (i.e., the contribution from the gas phase is negligible [$P_g = 0$]). Then for a small perturbation (denoted by primes) about the quiescent state (denoted by subscript 0), the solid-phase mass balance Equation 1 and momentum balance Equation 7 can be written, respectively, in their linearized form as

$$\begin{aligned} \{\acute{\varepsilon}_s\}_t + \varepsilon_{so} \{\acute{u}_s\}_x &= 0 \ , \\ \rho_s \varepsilon_{so} \{\acute{u}_s\}_t + G_o \{\acute{\varepsilon}_s\}_x &= 0 \ . \end{aligned} \tag{8}$$

Now differentiating the first with respect to x and the second with respect to t leads to

$$\{\acute{u}_s\}_{tt} - (G_o/\rho_s) \{\acute{u}_s\}_{xx} = 0 \ , \tag{9}$$

which is recognized as a wave equation with the speed of propagation given by

$$\sqrt{G_o/\rho_s} \ . \tag{10}$$

In the general, nonlinear case, the function G behaves as a "stiffness" modulus which is the product of density and propagation speed squared,

$$G(\varepsilon_s) = \rho_s a_s^2 \ . \tag{11}$$

In the theory underlying the XKTC code (Gough 1990), the constitutive assumption which defines the solid-phase stress tensor is embedded into the function G (Equation 11) by specifying a functional dependence of a_s. The propagation speed, a_s, is assigned as

$$a_s = a_1 \varepsilon_{g_o} / \varepsilon_g \quad \text{when loading ,}$$
$$= a_2 \quad \text{when unloading ,} \tag{12}$$

where the user-supplied constant, a_1, represents the speed of propagation during compressive loading when the bed is at the settling porosity, ε_{go}, and the constant a_2 represents the propagation speed during unloading from any state. Use of Equation 12 in Equation 11 effectively determines the dependence of σ_s on ε_s. To see this, recall the definition of G in Equation 5 which may be written as

$$\frac{d\sigma_s}{d\varepsilon_s} = G(\varepsilon_s) = \rho_s (a_1 \varepsilon_{g_o} / \varepsilon_g)^2 = -\frac{d\sigma_s}{d\varepsilon_g} . \tag{13}$$

A straightforward integration from ε_{go} to ε_g (during loading) yields the result

$$\sigma_s = \rho_s a_1^2 \varepsilon_{g_o}^2 \left(\frac{1}{\varepsilon_g} - \frac{1}{\varepsilon_{g_o}} \right) , \tag{14}$$

which Gough refers to as the "nominal loading curve." Note that specifying a value of a_1 uniquely determines σ_s as a function of porosity of the aggregate. Values of stress predicted by the nominal loading curve are sensitive to the value chosen for a_1, particularly when the aggregate is compressed to stress levels where porosity ε_g begins to vanish. More details of the derivation of Equation 14 may be found in Conroy (1992).

Wave structure in the two-phase mixture will be strongly influenced by the effective propagation speed in the mixture. This wave propagation speed can be predicted from a method-of-characteristics analysis of the two-phase equation system; the details are beyond the scope of this report but can be found in Gough (1974). In general, both solid and gas phases contribute to the value of this speed. However, the present study is concerned with the influence of the solid phase—before combustion generates a significant gas pressure. Accordingly, we will suppress the contribution of the gas phase by assuming a vanishingly

small gas pressure (e.g., a compressed aggregate under vacuum conditions). Under these special conditions, the effective speed of propagation in the mixture will be a_s given by Equation 12.

3. COMPRESSIBLE SOLID PHASE

Attempts to predict the transition to detonation in granular energetic material have led to the development of several two-phase model equation systems (Baer and Nunziato 1986; Kooker 1990) which account for a compressible solid phase. A major difference with an incompressible model is the addition of a solid-phase energy equation to track a variable internal energy along with the variable solid-phase density. Although the analysis by Kooker (1990) has not been used to simulate the interior ballistic cycle, this model assumes a strain-rate-independent equilibrium stress state for the compressed aggregate and, hence, should be capable of predicting the influence of solid propellant compressibility on wave speed. Again, the scope of the present study requires only a brief summary of some results from this model; details may be found in Kooker (1990).

Similar to the discussion of the Gough model above, assume here that the solid-phase stress tensor can be represented with the spherical component (a pressure), P_s. Now, however, P_s is a function of density ρ_s and specific internal energy e_s (i.e., $P_s(\rho_s, e_s)$). This function follows from the assumption that the Hugoniot for the *homogeneous solid material* can be described by a linear path in the shock velocity - particle velocity plane, i.e.,

$$\text{shock wave velocity} = b_{sh} + A_{sh} * \text{particle velocity} , \tag{15}$$

which leads to

$$P_s(\rho_s, e_s) = \rho_{s_o} \Gamma_o \left[\frac{e_s - e_{s_o}}{R+1}\right] + P_{s_o}\left[1 + \frac{\Gamma_o R}{R+1}\right] - \left(\frac{\rho_{s_o} b_{sh}^2}{2}\right)\left[2 + \frac{\Gamma_o R}{R+1}\right]\frac{R}{(1 + A_{sh} R)^2} \tag{16}$$

$$\text{where} \quad R \equiv (\rho_{s_o}/\rho_s) - 1 .$$

Based on this equation-of-state, the bulk sound speed in the *homogeneous solid material* is then

$$c_s^2 \equiv \frac{\partial P_s}{\partial \rho_s} + \left(\frac{P_s}{\rho_s^2} \right) \frac{\partial P_s}{\partial e_s} \, . \tag{17}$$

When the solid phase is assumed incompressible, changes in porosity (or solid volume fraction) of the mixture are predicted directly by the mass balance in Equation 1. However, when the solid phase is compressible, the mass balance becomes

$$\{ \rho_s \varepsilon_s \}_t + \{ \rho_s \varepsilon_s u_s \}_x = -\dot{m} \, , \tag{18}$$

which shows that changes in porosity and density are coupled. In the Kooker (1990) model, the additional equation required to determine both quantities is the constraint that the force balance at the interface between phases remains in equilibrium (also imposed in Gough's [1974, 1990] model)

$$P_s(\rho_s, e_s) - P_g(\rho_g, e_g) = \beta_s(\varepsilon_s) \, , \tag{19}$$

where β_s is the configuration stress (same as R_s in Gough's model) due to particle-particle contact when the granular solid phase is compacted into an aggregate. This rate-independent configuration stress is assumed to be a function of porosity as

$$\beta_s(\varepsilon_s) = \tau_1 [1 - \zeta^{p_1} + B_2 (\zeta^{-p_2} - 1)] \ln (1/\varepsilon_g) \, ,$$

$$\text{where} \quad \zeta \equiv (\varepsilon_g / \varepsilon_{g_o}) \, , \tag{20}$$

where the values of the parameters τ_1, p_1, p_2, and B_2 are determined by matching data from a quasi-static compaction experiment on the granular material of interest. The momentum balance for the solid phase will simply be Equation 3 with R_s replaced by β_s.

The effective wave propagation speed in this mixture is also a function of both the gas phase and the state of stress of the compacted aggregate. As in the case of Gough's (1974, 1990) model, the relationship follows from a method-of-characteristics analysis of the two-phase equation system (Kooker 1990). Under the same conditions postulated above for the Gough model (aggregate in hydrostatic stress, negligible gas pressure), the effective wave speed reduces to

$$a_K^2 = \left(\frac{\beta'_s + \beta_s / \varepsilon_s}{\beta'_s + \alpha_A} \right) c_s^2 ,$$

$$\text{where } \beta'_s \equiv \frac{d\beta_s}{d\varepsilon_s} ,$$

$$\text{and } \alpha_A \equiv \frac{\rho_s}{\varepsilon_s} \left[c_s^2 - \left(\frac{\beta_s}{\rho_s^2} \right) \frac{\partial P_s}{\partial e_s} \right] . \tag{21}$$

In the examples below, it is of interest to compute the "compressible" analog (denoted here as a_{sc}) to the incompressible speed, a_s, defined by $(G/\rho_s)^{1/2}$ as given in Equation 11. Recalling the definition of G in Equation 5 and with $\sigma_s = \varepsilon_s \beta_s$, then

$$a_{sc}^2 = \frac{G(\varepsilon_s)}{\rho_s} = \frac{d(\varepsilon_s \beta_s)/d\varepsilon_s}{\rho_s} , \tag{22}$$

where β_s is defined by Equation 20 and the values of ε_s and ρ_s must satisfy the equilibrium constraint in Equation 19.

4. DISCUSSION OF RESULTS

The analysis in Section 3 shows how the effective wave propagation speed in the mixture is influenced by the equilibrium stress state of the aggregate of compacted, granular gun propellant. Computation of numerical examples may provide a better assessment of this influence. Since the foundation of the prediction is the equilibrium stress state assigned to the mixture, the first step should be a comparison to data from full-scale, quasi-static compaction experiments on various granular gun propellants. At the present time, however, no such data exist in the stress range of interest. Some limited data at lower amplitudes, for example, have been reported by Robbins from 3-in-diameter cylindrical compression cell as described in Robbins and Conroy (1992). Some of these data for M30 propellant at room temperature are plotted in Figure 1 (Robbins and Conroy 1992) in the form of applied force vs. a gas porosity which is estimated from the observed volume change and the assumption of incompressibility. Figure 1 also

includes theoretical estimates of the applied load which follow from Grough's solid-phase stress function (Equation 14) for a range of assumed values for the aggregate wave speed at the settling porosity. Although a reasonable estimate for the wave speed at the settling porosity is a_1 = 175 m/s; in this case, Equation 14 does not lead to a good overall representation of the data. It is anticipated that full-scale, quasi-static compaction data obtained on gun propellants of interest will likely be similar to existing data for small granulation material. Typical compaction data displayed in Figure 2 represent two very different materials: Class D HMX is a brittle crystalline explosive (TMD of 1.903 g/cm^3) with an average particle diameter of 870 μm, and TS-3659 is a deformable double-base ball propellant (~21.6% NG in NC, TMD of 1.64 g/cm^3) with nearly spherical grains of 434 μm diameter. Details of the experiment and the data can be found in Elban and Chiarito (1986) for Class D HMX, and in Sandusky et al. (1988) for the TS-3659 ball propellant.

The smooth curves through the quasi-static compaction data shown in Figure 2 were determined by Kooker (1988, 1990) as "best fits" based on the assumed functional form for β_s in Equation 20 (65.3% TMD HMX: τ_1 - 1.0 K psi, p_1 = 0., B_2 - 0.79, p_2 = 1.22; 60% TMD TS-3659: τ_1 - 2.6 K psi, p_1 = 5.5, B_2 - 3.2, p_2 = 0.08). Note that in the early stage of compaction, the slope of the mixture stress curve is shallow for granular HMX which undergoes considerable grain fracture as the aggregate is compressed, while the slope for the deformable ball propellant is nearly uniform at a modest value. However, in the later stage of compaction for both materials, mixture stress increases steeply as the aggregates are compressed to densities near their respective TMD_o.

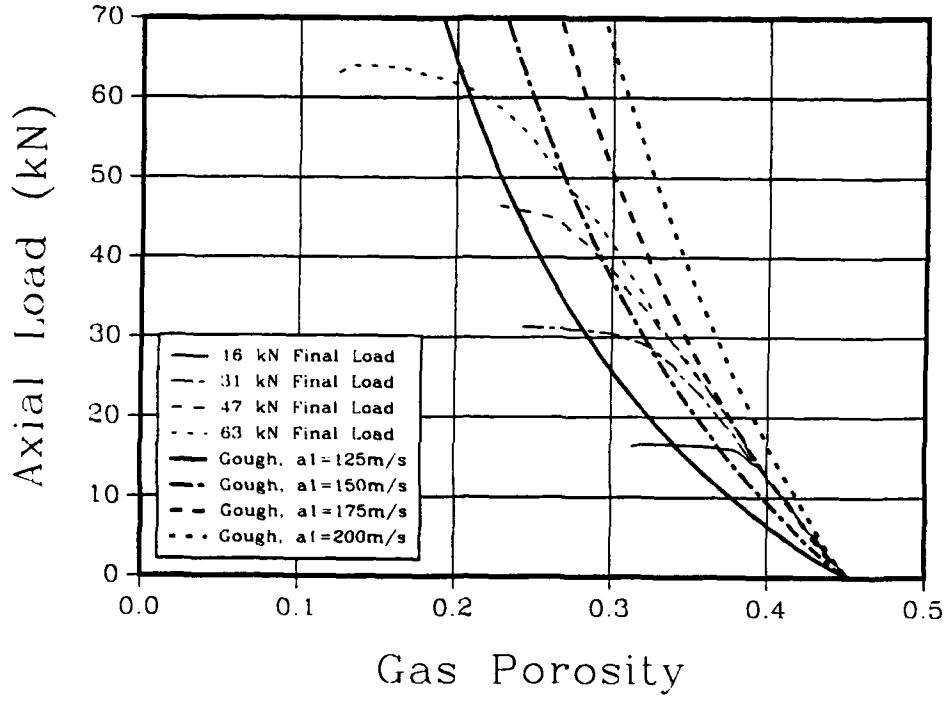

Figure 1. Four Experimental Compaction Curves (Robbins and Conroy 1992) for M30 Propellant at 294 K Compared to Gough's Description (Equation 14) for Values of a_1 Equal to 125, 150, 175, and 200 m/s.

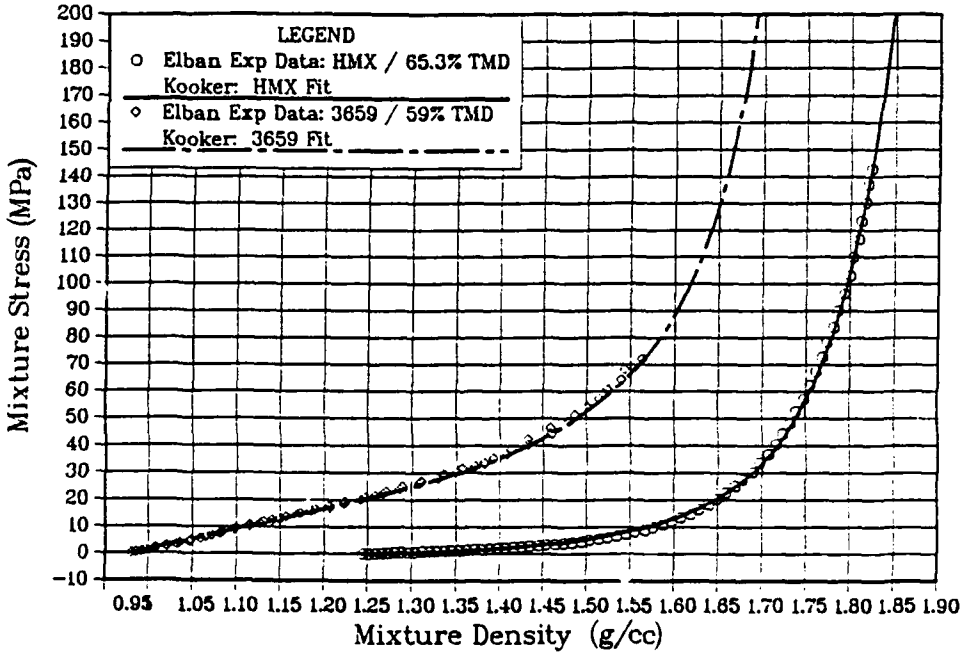

Figure 2. Quasi-Static Compaction Data for Two Granular Materials: (a) 65.3% TMD Class D HMX, 870 μm Diameter, TMD_o = 1.903 g/cm^3 (Elban and Chiarito 1986), (b) 59% TMD TS-3659 Double-Base Ball Propellant, 434 μm Diameter, TMD_o = 1.64 g/cm^3 (Sandusky et al. 1988).

If the quasi-static compaction data in Figure 2 represented actual gun propellant, then an XKTC (1990) simulation would first require that the nominal loading curve of Equation 14 be used to described the data. As an example here, choose the HMX data which is reproduced in Figure 3. Also shown in Figure 3 are the three curves which follow from Equation 14 when a_1 is chosen to be 100, 200, and 300 m/s. Note that in the early stages of compaction, the slope of the experimental data is well approximated by the curve based on a_1 = 100 m/s, but in the later stages the value of an "effective" a_1 increases. Although σ_s given by Equation 14 is not a good approximation for the HMX data, it must be remembered that Gough chose this functional dependence over 15 years ago without the benefit of any experimental data. From that perspective, his choice was remarkably insightful.

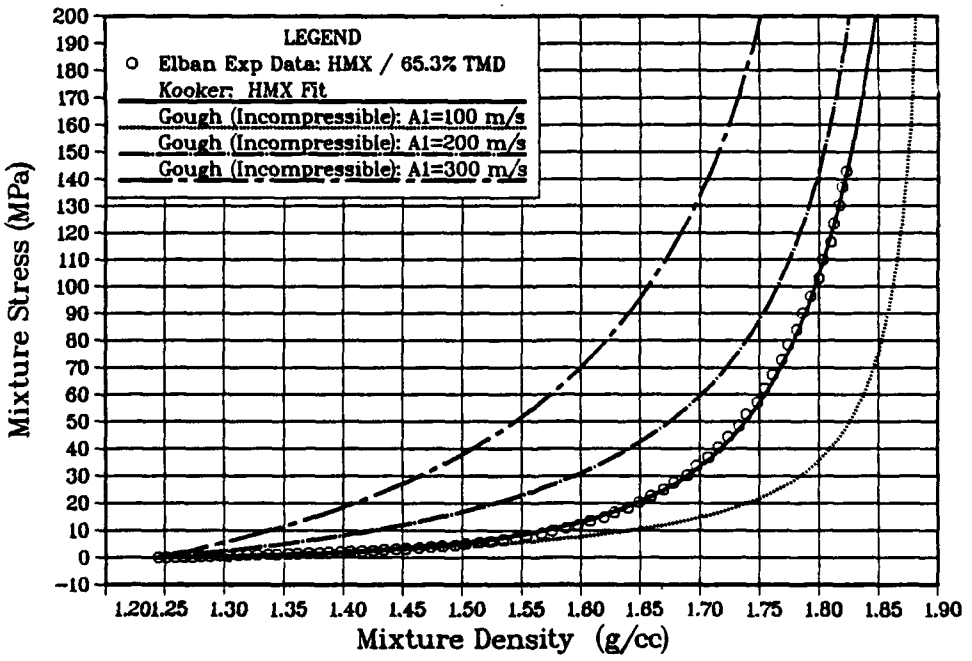

Figure 3. Mixture Stress vs. Mixture Density for Isothermal Quasi-Static Compaction of 65.3% TMD Class D HMX. Data From Elban and Chiarito (1986); Solid Curve Is "Best-Fit" by Kooker (1988). Other Curves From Gough's Formulation (Equation 14) With Values of a_1 From 100–300 m/s.

Predictions for mixture wave speed (intentionally neglecting the contribution from the gas phase) are shown in Figure 4, where the solid line follows from Equation 21 and the compressible analysis. All the estimates concur that the effective propagation speed increases substantially as the porosity of the mixture begins to vanish (i.e., mixture density approaches that of the TMD solid). As a result of the fit to the quasi-static compaction data, Gough's incompressible analysis (chain-dot curve from Equation 12) with a_1 = 100 m/s increases slowly but then rises quite abruptly as mixture density approaches TMD_o of 1.903 g/cm^3. Retaining the same basic assumptions but representing the experimental data for σ_s with the solid line shown in Figure 3 produces the "dotted" curve in Figure 4. Using the same basic structure (i.e., Equation 22) but replacing ρ_s and ε_s with the "compressible" values which are roots of Equation 19, leads to the chain-dash curve shown in Figure 4. This curve is a reasonable approximation to the compressible behavior up to a mixture density of 1.8 g/cm^3. At mixture densities greater than 1.8 g/cm^3 in Figure 4, the incompressible estimates diverge significantly from the compressible prediction.

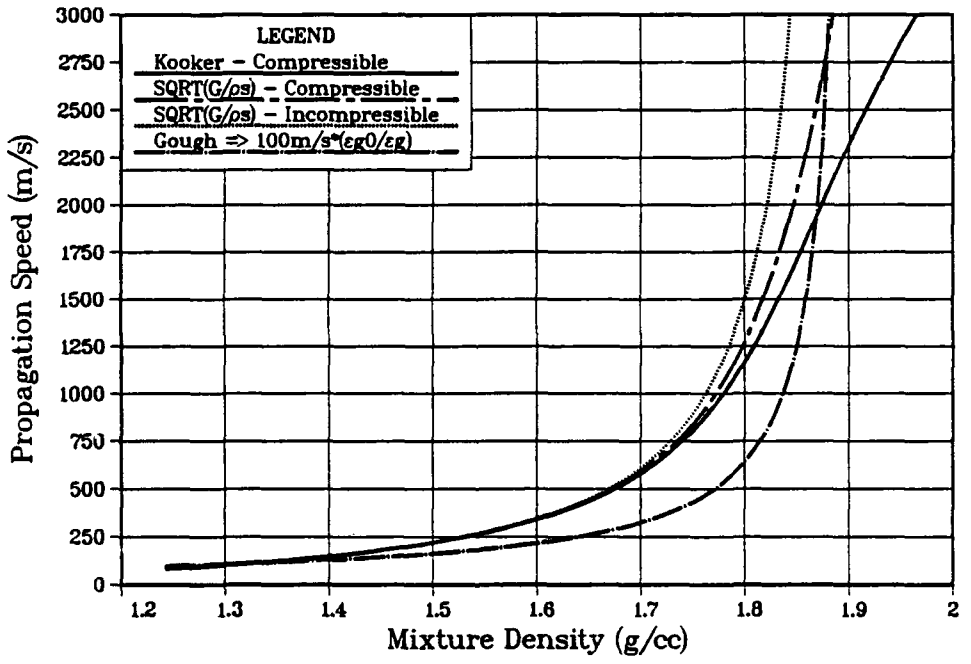

Figure 4. Effective Wave Propagation Speed in 65.3% TMD Class D HMX During Isothermal Compression (With P_g = 0). Solid Curve From (Equation 21) Assuming Compressible Solid Phase; Chain-Dot Curve From Gough (Equation 12) With a_1 = 100 m/s; Dotted Curve Is Incompressible $(G/\rho_s)^{1/2}$; Chain-Dash Curve Is Compressible $(G/\rho_s)^{1/2}$ or a_{sc} From Equation 22.

Figure 5 gives a clearer picture of the change in behavior. At low density, the mixture propagation speed is controlled by the fundamental compaction characteristics of the granular aggregate which are closely approximated by a_{sc} (chain-dash curve in Figure 5) given by Equation 22. At high density, most of the porosity has been eliminated and/or the aggregate has "locked" such that the mixture propagation speed is dominated by the compressibility of the homogeneous material itself (dotted curve in Figure 5). The compressible prediction given by Equation 21 transitions between these two limits.

The implication of these results may be easier to visualize by plotting mixture propagation speed as a function of mixture stress, as shown in Figure 6. For the present example at values of mixture stress below 50 MPa, there is little difference among the predictions from the various methods. Important differences appear near stress levels of 100 MPa. And at 200 MPa, there is a dramatic divergence such that the incompressible result is nearly a factor of two greater than the compressible prediction. In general, as the effective wave speed is reduced, increases in mixture stress are more likely to propagate as shock waves. However, a more detailed investigation involving simulations will be required to predict the influence on the behavior in a gun combustion chamber.

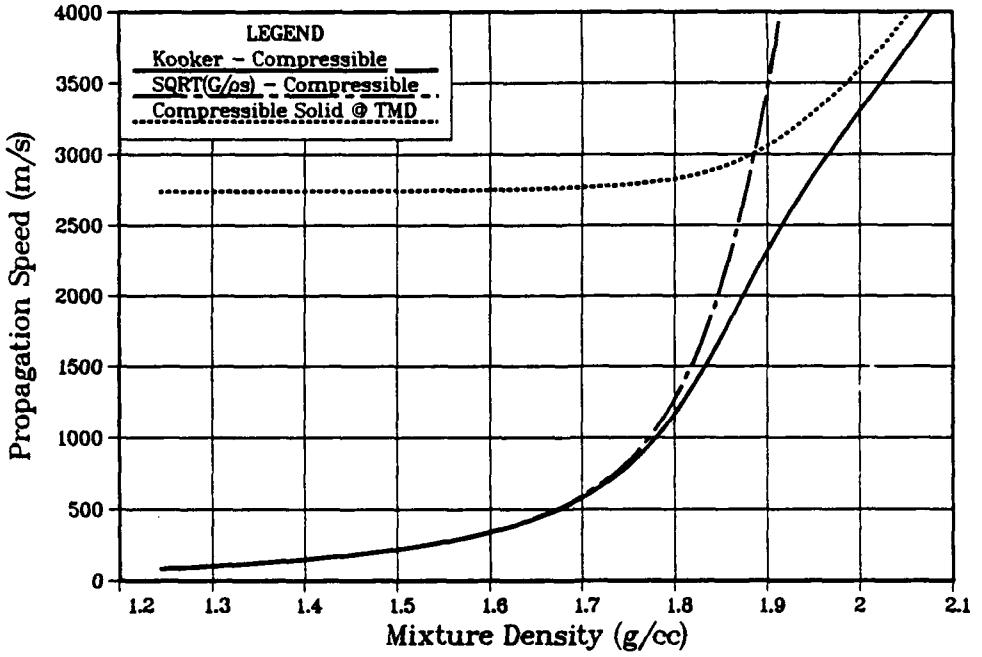

Figure 5. Effective Wave Propagation Speed in 65.3% TMD Class D HMX During Isothermal Compression (With $P_g = 0$). Solid Curve From Equation 21 Assuming Compressible Solid Phase; Chain-Dash Curve Is Compressible $(G/\rho_s)^{1/2}$ or a_{sc} From Equation 22; Dotted Curve Is Bulk Sound Speed in Homogeneous Solid (Equation 17).

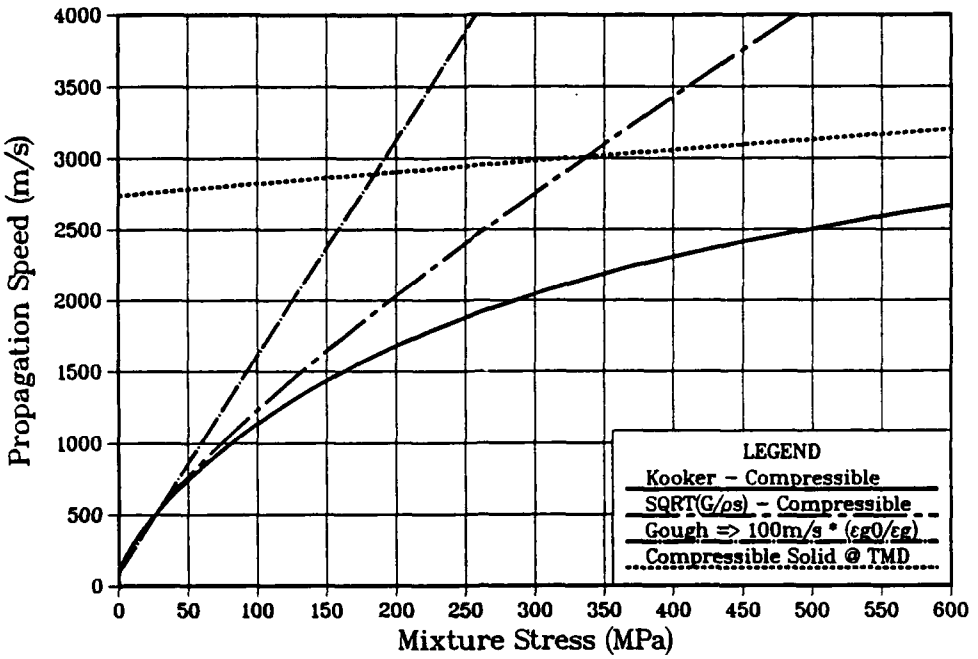

Figure 6. Effective Wave Propagation Speed vs. Mixture Stress in 65.3% TMD Class D HMX During Isothermal Compression (With $P_g = 0$). Solid Curve From Equation 21 Assuming Compressible Solid Phase; Chain-Dash Curve Is Compressible $(G/\rho_s)^{1/2}$ or a_{sc} From Equation 22; Chain-Dot Curve From Gough (Equation 12) With $a_1 = 100$ m/s.

A similar analysis and comparison was made for the double-base ball propellant TS-3659. The experimental data from quasi-static compaction shown in Figure 2 is reproduced in Figure 7 along with three curves which follow from Equation 14 when a_1 is chosen to be 100, 200, and 300 m/s. Comparison shows that the "effective" value of a_1 would have to decrease considerably from its initial value of approximately 250 m/s; the experimental data are not well represented by Equation 14. Again, this illustrates that even a good estimate of the compacted bed wave speed at the settling porosity does not ensure that the mixture stress behavior has been captured.

Predictions for wave propagation speed in TS-3659 are displayed in Figure 8, where again the dotted curve follows from the incompressible prediction similar to Gough's analysis but with σ_s given by the experimental data, the chain-dashed curve follows from a_{sc} in Equation 22 which incorporates the compressible correction for ρ_s and ε_s, and the solid curve follows the compressible analysis and Equation 21. The results are similar to those for the HMX case.

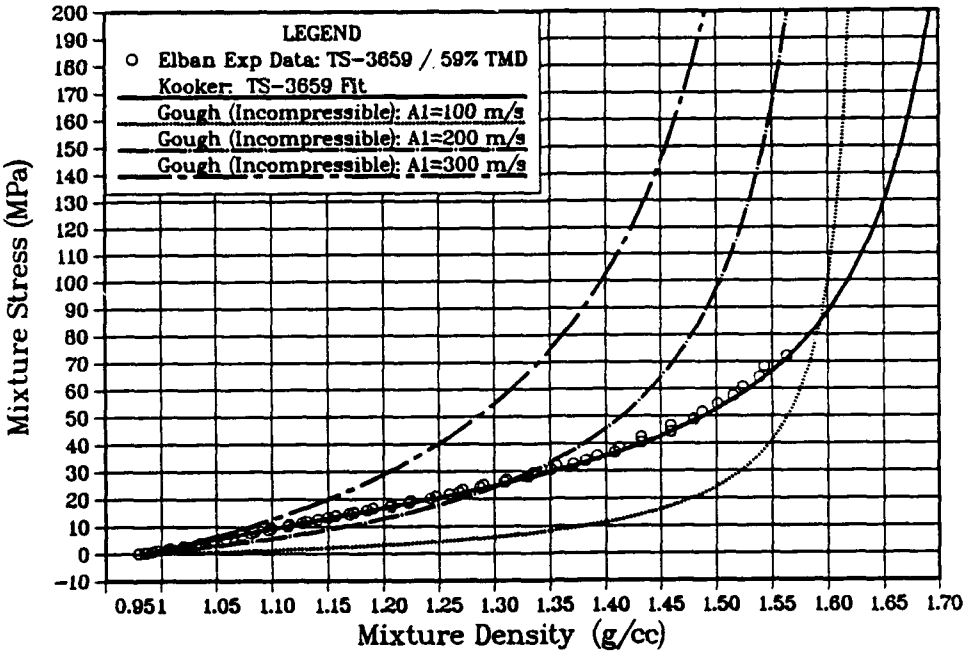

Figure 7. Mixture Stress vs. Mixture Density for Isothermal Quasi-Static Compaction of 59% TMD TS-3659 Double-Base Ball Propellant. Data From Sandusky et al. (1988); Solid Curve is "Best-Fit" by Kooker (1990). Other Curves From Gough's Formulation (Equation 14) With Values of a_1 From 100–300 m/s.

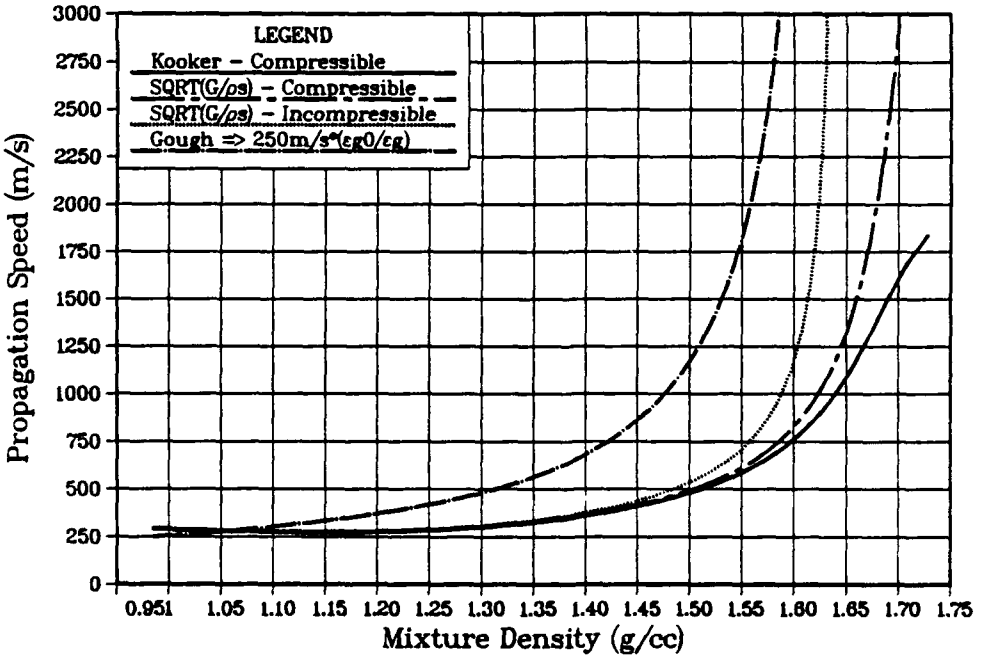

Figure 8. Effective Wave Propagation Speed in 60% TMD TS-3659 Double-Base Ball Propellant During Isothermal Compression (With $P_s = 0$). Solid Curve From Equation 21 Assuming Compressible Solid Phase; Chain-Dot Curve From Gough (Equation 12) With $a_1 = 250$ m/s; Dotted Curve Is Incompressible $(G/\rho_s)^{1/2}$; Chain-Dash Curve Is Compressible $(G/\rho_s)^{1/2}$ or a_{sc} From Equation 22.

5. CONCLUSIONS

All current interior ballistic calculations are based on mixture theories which require a phenomenological submodel to relate porosity of the compacted aggregate of propellant grains to a stress state. The accuracy of any simulation showing the growth of pressure waves to potentially dangerous amplitudes will depend upon the accuracy of the constitutive behavior assigned to the compacted aggregate. The current formulation in the XKTC (Gough 1990) code assumes an incompressible solid phase and a strain-rate independent relationship which is uniquely defined by a value of mixture wave speed (a_1) at the settling porosity. Comparison to data from small-scale, quasi-static compression experiments indicates that an improvement might be expected from a direct representation of the data. Estimates of the effective wave propagation speed in the mixture (with the restriction of vanishing gas pressure) show the potential importance of including compressibility of the solid phase when mixture stress approaches the level of 100 MPa. Accounting for solid-phase compressibility within the current interior ballistic models would require a major restructuring. However, a reasonable compromise might be to alter the predicted incompressible wave speed with a correction for compressibility.

INTENTIONALLY LEFT BLANK.

6. REFERENCES

Baer, M. R., and J. W. Nunziato. "A Two-Phase Mixture Theory for the Deflagration-to-Detonation Transition (DDT) in Reactive Granular Materials." International Journal of Multiphase Flow, vol. 12, no. 6, pp. 861–889, 1986.

Conroy, P. J. "Rheological Formulation of the NOVA Family of Interior Ballistic Codes." U.S. Army Ballistic Research Laboratory, Aberdeen Proving Ground, MD, to be published.

Conroy, P. J. "Rheological Studies Related to Interior Ballistics: A Historical Perspective." BRL-MR-3970, U.S. Army Ballistic Research Laboratory, Aberdeen Proving Ground, MD, May 1992.

Elban, W. L. "Quasi-Static Compaction Studies for DDT Investigations." Propellants, Explosives, Pyrotechnics, vol. 9, pp. 119–129, 1984.

Elban, W. L., and M. A. Chiarito. "Quasi-Static Compaction Study of Coarse HMX Explosive." Powder Technology, vol. 46, pp. 181–193, 1986.

Gazonas, G. A., A. Juhasz, and J. C. Ford. "Strain Rate Insensitivity of Damage-Induced Surface Area in M30 and JA2 Gun Propellants." BRL-TR-3251, U.S. Army Ballistic Research Laboratory, Aberdeen Proving Ground, MD, August 1991.

Gazonas, G. A. "The Mechanical Response of M30, XM39, and JA2 Propellants at Strain Rates from 10^{-2} to 250 sec^{-1}". BRL-TR-3181, U.S. Army Ballistic Research Laboratory, Aberdeen Proving GRound, MD, January 1991.

Gough, P. S. "The Flow of a Compressible Gas Through an Aggregate of Mobile Reacting Particles." IHCR 80-7, Naval Ordnance Station, Indian Head, MD, 30 December 1980 (reprint of Gough's Ph.D Thesis, Department of Mechanical Engineering, McGill University, December 1974).

Gough, P. S. "The XNOVAKTC Code." PGA-TR-86-1, Paul Gough Associates, Portsmouth, N.H., March 1986; see also BRL-CR-627, U.S. Army Ballistic Research Laboratory, Aberdeen Proving Ground, MD, February 1990, and IHCR 80-8, vol. I, Naval Ordnance Station, Indian Head, MD, 30 December 1980.

Kooker, D. E. "Modeling of Compaction Wave Behavior in Confined Granular Energetic Material." BRL-TR-3138, U.S. Army Ballistic Research Laboratory, Aberdeen Proving Ground, MD, August 1990.

Kooker, D. E. "A Reactive Shock Wave Model for Compaction Waves in Granular Energetic Material." BRL-TR-2945, U.S. Army Ballistic Research Laboratory, Aberdeen Proving Ground, MD, November 1988.

Lieb, R. J., and J. J. Rocchio. "High Strain Rate Mechanical Properties Testing on Lots of Gun Propellant With Deviant Interior Ballistic Performance." Proceedings of the 1982 JANNAF Structures and Mechanical Behavior Subcommittee Meeting, CPIA Pub. 368, pp. 23–38, October 1982.

Lieb, R. J. "The Mechanical Response of M30, JA2 and XM39 Gun Propellants to High-Rate Deformation." BRL-TR-3023, U.S. Army Ballistic Research Laboratory, Aberdeen Proving Ground, MD, August 1989.

Lieb, R. J. "High Strain Rate Response of Gun Propellant Using the Hopkinson Split Bar." BRL-TR-3200, U.S. Army Ballistic Research Laboratory, Aberdeen Proving Ground, MD, February 1991.

Lieb, R. J. and M. G. Leadore. "Mechanical Failure Parameters in Gun Propellants." BRL-TR-3296, U.S. Army Ballistic Research Laboratory, Aberdeen Proving Ground, MD, November 1991.

Lieb, R. J. and M. G. Leadore. "Mechanical Response Comparison of Gun Propellants Evaluated Under Equivalent Time-Temperature Conditions." Proceedings of the JANNAF Structures and Mechanical Behavior Subcommittee Meeting, 16-60 November 1992.

Nicolaides, S., D. A. Wiegand, and J. Pinto. "The Mechanical Behavior of Gun Propellant Grains and its Role in Interior Ballistics." Proceedings of the 16th JANNAF Structures and Mechanical Behavior Subcommittee Meeting, CPIA Pub. 311, pp. 145–165, 1980.

Robbins, F. W., and P. J. Conroy. "Rheological Studies on M30 Propellant." BRL-TR-3205, U.S. Army Ballistic Research Laboratory, Aberdeen Proving Ground, MD, February 1991.

Sandusky, H. W., B. C. Glancy, R. L. Campbell, A. D. Krall, W. L. Elban, and P. J. Coyne, Jr. "Compaction and Compressive Reaction Studies for a Spherical, Double-Base Ball Propellant." Proceedings of the 25th JANNAF Combustion Meeting, CPIA Pub. 498, vol. I, pp. 83–94, October 1988.

LIST OF SYMBOLS

A_{sh} = slope of Hugoniot for homogeneous solid material (see Equation 15)

a_1 = wave propagation speed in packed bed during compressive loading, when $\varepsilon_g = \varepsilon_{go}$

a_2 = wave propagation speed in packed bed during unloading

a_K = "compressible" wave propagation speed (see Equation 21)

a_s = wave propagation speed in packed bed (see Equation 12)

a_{sc} = wave propagation speed defined in Equation 22

b_{sh} = intercept of Hugoniot for homogeneous solid material (see Equation 15)

B_2 = parameter (n-d) in expression for β_s (see Equation 20)

c_s = bulk sound speed in homogeneous solid material (see Equation 17)

f_d = interphase drag force per unit total volume

G = $d\sigma_s/d\varepsilon_s$ as defined in Equation 5

G_o = $d\sigma_s/d\varepsilon_{s_o}$ evaluated at the settling porosityn $\varepsilon_g o$

$\dot{m}$ = mass generation rate of gas (due to pyrolysis or combustion of solid) per unit total volume

p_1 and p_2 = parameters (n-d) in expression for β_s (see Equation 20)

P_g = static pressure in gas phase

P_s = spherical stress {pressure} in solid phase

R_s = $P_s - P_g$ = configuration stress in Gough's analysis

TMD = theoretical maximum density (TMD_o => at atmospheric pressure)

u_s = velocity of the solid phase

β_s = configuration stress of packed bed = intrinsic average intergranular stress

Γ_o = Mie Gruneisen coefficient (assumed constant here)

ε_s = solid volume fraction = solid volume/total volume

ε_g = gas porosity = $1 - \varepsilon_s$ = gas volume/total volume

ρ_s = solid-phase density = mass of solid/solid volume

σ_s = $\varepsilon_s \beta_s$ = non-intrinsic average granular stress

x = spacial coordinate

$\{\ \}_x$ = partial derivative with respect to space coordinate

$\{\ \}_{xx}$ = second partial derivative with respect to space coordinate

t = time

$\{\ \}_t$ = partial derivative with respect to time

$\{\ \}_{tt}$ = second partial derivative with respect to time

$\acute{\varepsilon}_s$ = small variance of the solid volume fraction about a quiescent state

$\acute{u}_s$ = small variance of the velocity about a quiescent state

ε_{s_o} = settling solid volume fraction

ε_{g_o} = $1 - \varepsilon_{s_o}$

ε_g = $1 - \varepsilon_s$

$\frac{D}{Dt_s}$ = substantial derivative along solid-phase streamline = $\{\ \}_t + u_s \{\ \}_x$

e_s = solid phase energy

e_{s_o} = solid phase energy at the settling porosity

No. of Copies	Organization
2	Administrator Defense Technical Info Center ATTN: DTIC-DDA Cameron Station Alexandria, VA 22304-6145
1	Commander U.S. Army Materiel Command ATTN: AMCAM 5001 Eisenhower Ave. Alexandria, VA 22333-0001
1	Director U.S. Army Research Laboratory ATTN: AMSRL-D 2800 Powder Mill Rd. Adelphi, MD 20783-1145
1	Director U.S. Army Research Laboratory ATTN: AMSRL-OP-CI-AD, Tech Publishing 2800 Powder Mill Rd. Adelphi, MD 20783-1145
2	Commander U.S. Army Armament Research, Development, and Engineering Center ATTN: SMCAR-IMI-I Picatinny Arsenal, NJ 07806-5000
2	Commander U.S. Army Armament Research, Development, and Engineering Center ATTN: SMCAR-TDC Picatinny Arsenal, NJ 07806-5000
1	Director Benet Weapons Laboratory U.S. Army Armament Research, Development, and Engineering Center ATTN: SMCAR-CCB-TL Watervliet, NY 12189-4050
(Unclass. only)1	Commander U.S. Army Rock Island Arsenal ATTN: SMCRI-IMC-RT/Technical Library Rock Island, IL 61299-5000
1	Director U.S. Army Aviation Research and Technology Activity ATTN: SAVRT-R (Library) M/S 219-3 Ames Research Center Moffett Field, CA 94035-1000

No. of Copies	Organization
1	Commander U.S. Army Missile Command ATTN: AMSMI-RD-CS-R (DOC) Redstone Arsenal, AL 35898-5010
1	Commander U.S. Army Tank-Automotive Command ATTN: ASQNC-TAC-DIT (Technical Information Center) Warren, MI 48397-5000
1	Director U.S. Army TRADOC Analysis Command ATTN: ATRC-WSR White Sands Missile Range, NM 88002-5502
1	Commandant U.S. Army Field Artillery School ATTN: ATSF-CSI Ft. Sill, OK 73503-5000
(Class. only)1	Commandant U.S. Army Infantry School ATTN: ATSH-CD (Security Mgr.) Fort Benning, GA 31905-5660
(Unclass. only)1	Commandant U.S. Army Infantry School ATTN: ATSH-CD-CSO-OR Fort Benning, GA 31905-5660
1	WL/MNOI Eglin AFB, FL 32542-5000
	Aberdeen Proving Ground
2	Dir, USAMSAA ATTN: AMXSY-D AMXSY-MP, H. Cohen
1	Cdr, USATECOM ATTN: AMSTE-TC
1	Dir, ERDEC ATTN: SCBRD-RT
1	Cdr, CBDA ATTN: AMSCB-CI
1	Dir, USARL ATTN: AMSRL-SL-I
10	Dir, USARL ATTN: AMSRL-OP-CI-B (Tech Lib)

No. of Copies	Organization
1	Chairman DOD Explosives Safety Board Room 856-C Hoffman Bldg. 1 2461 Eisenhower Avenue Alexandria, VA 22331-0600
1	Headquarters U.S. Army Materiel Command ATTN: AMCICP-AD, M. Fisette 5001 Eisenhower Ave. Alexandria, VA 22333-0001
1	U.S. Army Ballistic Missile Defense Systems Command Advanced Technology Center P.O. Box 1500 Huntsville, AL 35807-3801
1	Department of the Army Office of the Product Manager 155mm Howitzer, M109A6, Paladin ATTN: SFAE-AR-HIP-IP, Mr. R. De Kleine Picatinny Arsenal, NJ 07806-5000
3	Project Manager Advanced Field Artillery System ATTN: SFAE-ASM-AF-E LTC D. Ellis T. Kuriata J. Shields Picatinny Arsenal, NJ 07801-5000
1	Project Manager Advanced Field Artillery System ATTN: SFAE-ASM-AF-Q, W. Warren Picatinny Arsenal, NJ 07801-5000
2	Commander Production Base Modernization Agency U.S. Army Armament Research, Development, and Engineering Center ATTN: AMSMC-PBM, A. Siklosi AMSMC-PBM-E, L. Laibson Picatinny Arsenal, NJ 07806-5000
4	PEO-Armaments Project Manager Tank Main Armament System ATTN: AMCPM-TMA AMCPM-TMA-105 AMCPM-TMA-120 AMCPM-TMA-AS, H. Yuen Picatinny Arsenal, NJ 07806-5000
5	Commander U.S. Army Armament Research, Development, and Engineering Center ATTN: SMCAR-CCD, D. Spring SMCAR-CCH-V, C. Mandala E. Fennell SMCAR-CCH-T, L. Rosendorf SMCAR-CCS Picatinny Arsenal, NJ 07806-5000
19	Commander U.S. Army Armament Research, Development, and Engineering Center ATTN: SMCAR-AEE, J. Lannon SMCAR-AEE-B, A. Beardell D. Downs S. Einstein S. Westley S. Bernstein J. Rutkowski B. Brodman P. O'Reilly R. Cirincione A. Grabowsky P. Hui J. O'Reilly SMCAR-AEE-WW, M. Mezger J. Pinto D. Wiegand P. Lu C. Hu SMCAR-AES, S. Kaplowitz Picatinny Arsenal, NJ 07806-5000
1	Commander U.S. Army Armament Research, Development and Engineering Center ATTN: SMCAR-HFM, E. Barrieres Picatinny Arsenal, NJ 07806-5000

No. of Copies | Organization

9 Commander
U.S. Army Armament Research, Development and Engineering Center
ATTN: SMCAR-FSA-T, M. Salsbury
SMCAR-FSA-F, LTC R. Riddle
SMCAR-FSC, G. Ferdinand
SMCAR-FS, T. Gora
SMCAR-FS-DH, J. Feneck
SMCAR-FSS-A, R. Kopman
B. Machek
L. Pinder
SMCAR-FSN-N, K. Chung
Picatinny Arsenal, NJ 07806-5000

3 Director
Benet Weapons Laboratories
ATTN: SMCAR-CCB-RA,
G.P. O'Hara
G.A. Pflegl
SMCAR-CCB-S, F. Heiser
Watervliet, NY 12189-4050

2 Commander
U.S. Army Research Office
ATTN: Technical Library
D. Mann
P.O. Box 12211
Research Triangle Park, NC 27709-2211

1 Commander, USACECOM
R&D Technical Library
ATTN: ASQNC-ELC-IS-L-R,
Myer Center
Fort Monmouth, NJ 07703-5301

1 Commander
U.S. Army Harry Diamond Laboratory
ATTN: SLCHD-TA-L
2800 Powder Mill Rd.
Adelphi, MD 20783-1145

1 Commandant
U.S. Army Aviation School
ATTN: Aviation Agency
Fort Rucker, AL 36360

1 Program Manager
U.S. Tank-Automotive Command
ATTN: AMCPM-ABMS, T. Dean
Warren, MI 48092-2498

No. of Copies | Organization

1 Project Manager
U.S. Tank-Automotive Command
Fighting Vehicle Systems
ATTN: SFAE-ASM-BV
Warren, MI 48397-5000

1 Project Manager, Abrams Tank System
ATTN: SFAE-ASM-AB
Warren, MI 48397-5000

1 Director
HQ, TRAC RPD
ATTN: ATCD-MA
Fort Monroe, VA 23651-5143

2 Director
U.S. Army Materials Technology Laboratory
ATTN: SLCMT-ATL (2 cps)
Watertown, MA 02172-0001

1 Commander
U.S. Army Belvoir Research and Development Center
ATTN: STRBE-WC
Fort Belvoir, VA 22060-5006

1 Director
U.S. Army TRAC-Ft. Lee
ATTN: ATRC-L, Mr. Cameron
Fort Lee, VA 23801-6140

1 Commandant
U.S. Army Command and General Staff College
Fort Leavenworth, KS 66027

1 Commandant
U.S. Army Special Warfare School
ATTN: Rev and Trng Lit Div
Fort Bragg, NC 28307

1 Commander
Radford Army Ammunition Plant
ATTN: SMCAR-QA/HI LIB
Radford, VA 24141-0298

No. of Copies | Organization

1 Commander
U.S. Army Foreign Science and Technology Center
ATTN: AMXST-MC-3
220 Seventh Street, NE
Charlottesville, VA 22901-5396

2 Commandant
U.S. Army Field Artillery Center and School
ATTN: ATSF-CO-MW, E. Dublisky
ATSF-CN, P. Gross
Ft. Sill, OK 73503-5600

1 Commandant
U.S. Army Armor School
ATTN: ATZK-CD-MS, M. Falkovitch
Armor Agency
Fort Knox, KY 40121-5215

2 Commander
Naval Sea Systems Command
ATTN: SEA 62R
SEA 64
Washington, DC 20362-5101

1 Commander
Naval Air Systems Command
ATTN: AIR-954-Tech Library
Washington, DC 20360

4 Commander
Naval Research Laboratory
ATTN: Technical Library
Code 4410, K. Kailasanate
J. Boris
E. Oran
Washington, DC 20375-5000

1 Office of Naval Research
ATTN: Code 473, R.S. Miller
800 N. Quincy Street
Arlington, VA 22217-9999

1 Office of Naval Technology
ATTN: ONT-213, D. Siegel
800 N. Quincy St.
Arlington, VA 22217-5000

No. of Copies | Organization

4 Commander
Naval Surface Warfare Center
ATTN: Code 730
Code R-13,
R. Bernecker
H. Sandusky
Silver Spring, MD 20903-5000

7 Commander
Naval Surface Warfare Center
ATTN: T.C. Smith
K. Rice
S. Mitchell
S. Peters
J. Consaga
C. Gotzmer
Technical Library
Indian Head, MD 20640-5000

5 Commander
Naval Surface Warfare Center
ATTN: Code G30,
Code G32,
Code G33, J.L. East
T. Doran
Code E23 Technical Library
Dahlgren, VA 22448-5000

5 Commander
Naval Air Warfare Center
ATTN: Code 388, C.F. Price
T. Boggs
Code 3895, T. Parr
R. Derr
Information Science Division
China Lake, CA 93555-6001

2 Commanding Officer
Naval Underwater Systems Center
ATTN: Code 5B331, R.S. Lazar
Technical Library
Newport, RI 02840

1 AFOSR/NA
ATTN: J. Tishkoff
Bolling AFB, D.C. 20332-6448

1 OLAC PL/TSTL
ATTN: D. Shiplett
Edwards AFB, CA 93523-5000

No. of Copies	Organization
3	AL/LSCF ATTN: J. Levine L. Quinn T. Edwards Edwards AFB, CA 93523-5000
1	WL/MNAA ATTN: B. Simpson Eglin AFB, FL 32542-5434
1	WL/MNME Energetic Materials Branch 2306 Perimeter Rd. STE 9 Eglin AFB, FL 32542-5910
1	WL/MNSH ATTN: R. Drabczuk Eglin AFB, FL 32542-5434
2	NASA Langley Research Center ATTN: M.S. 408, W. Scallion D. Witcofski Hampton, VA 23605
1	Central Intelligence Agency Office of the Central References Dissemination Branch Room GE-47, HQS Washington, DC 20502
1	Central Intelligence Agency ATTN: J. Backofen NHB, Room 5N01 Washington, DC 20505
1	SDIO/TNI ATTN: L.H. Caveny Pentagon Washington, DC 20301-7100
1	SDIO/DA ATTN: E. Gerry Pentagon Washington, DC 21301-7100
2	HQ DNA ATTN: D. Lewis A. Fahey 6801 Telegraph Rd. Alexandria, VA 22310-3398

No. of Copies	Organization
1	Director Sandia National Laboratories Energetic Materials & Fluid Mechanics Department, 1512 ATTN: M. Baer P.O. Box 5800 Albuquerque, NM 87185
1	Director Sandia National Laboratories Combustion Research Facility ATTN: R. Carling Livermore, CA 94551-0469
4	Director Lawrence Livermore National Laboratory ATTN: L-355, A. Buckingham G. Benedetti M. Finger L-324, M. Constantino P.O. Box 808 Livermore, CA 94550-0622
2	Director Los Alamos Scientific Lab ATTN: T3/D. Butler M. Division/B. Craig P.O. Box 1663 Los Alamos, NM 87544
3	Battelle Columbus Laboratories ATTN: TACTEC Library, J.N. Huggins V. Levin 505 King Avenue Columbus, OH 43201-2693
1	Battelle PNL ATTN: Mr. Mark Garnich P.O. Box 999 Richland, WA 99352
1	Institute of Gas Technology ATTN: D. Gidaspow 3424 S. State Street Chicago, IL 60616-3896

No. of Copies	Organization
1	Institute for Advanced Technology ATTN: T.M. Krehne The University of Texas of Austin 4030-2 W. Braker Lane Austin, TX 78759-5329
2	CPIA - JHU ATTN: Hary J. Hoffman T. Christian 10630 Little Patuxent Parkway Suite 202 Columbia, MD 21044-3200
1	Brigham Young University Department of Chemical Engineering ATTN: M. Beckstead Provo, UT 84601
1	Jet Propulsion Laboratory California Institute of Technology ATTN: L.D. Strand, MS 125/224 4800 Oak Grove Drive Pasadena, CA 91109
1	California Institute of Technology 204 Karman Lab Main Stop 301-46 ATTN: F.E.C. Culick 1201 E. California Street Pasadena, CA 91109
3	Georgia Institute of Technology School of Aerospace Engineering ATTN: B.T. Zim E. Price W.C. Strahle Atlanta, GA 30332
1	Massachusetts Institute of Technology Department of Mechanical Engineering ATTN: T. Toong 77 Massachusetts Avenue Cambridge, MA 02139-4307
1	University of Illinois Department of Mechanical/Industry Engineering ATTN: H. Krier 144 MEB; 1206 N. Green St. Urbana, IL 61801-2978

No. of Copies	Organization
1	University of Maryland ATTN: Dr. J.D. Anderson College Park, MD 20740
1	University of Massachusetts Department of Mechanical Engineering ATTN: K. Jakus Amherst, MA 01002-0014
1	University of Minnesota Department of Mechanical Engineering ATTN: E. Fletcher Minneapolis, MN 55414-3368
3	Pennsylvania State University Department of Mechanical Engineering ATTN: V. Yang K. Kuo C. Merkle University Park, PA 16802-7501
1	Rensselaer Polytechnic Institute Department of Mathematics Troy, NY 12181
1	Stevens Institute of Technology Davidson Laboratory ATTN: R. McAlevy III Castle Point Station Hoboken, NJ 07030-5907
1	Rutgers University Department of Mechanical and Aerospace Engineering ATTN: S. Temkin University Heights Campus New Brunswick, NJ 08903
1	University of Southern California Mechanical Engineering Department ATTN: 0HE200, M. Gerstein Los Angeles, CA 90089-5199
1	University of Utah Department of Chemical Engineering ATTN: A. Baer Salt Lake City, UT 84112-1194
1	Washington State University Department of Mechanical Engineering ATTN: C.T. Crowe Pullman, WA 99163-5201

No. of Copies	Organization
1	AFELM, The Rand Corporation ATTN: Library D 1700 Main Street Santa Monica, CA 90401-3297
1	Arrow Technology Associates, Inc. ATTN: W. Hathaway P.O. Box 4218 South Burlington, VT 05401-0042
3	AAI Corporation ATTN: J. Hebert J. Frankle D. Cleveland P.O. Box 126 Hunt Valley, MD 21030-0126
2	Alliant Techsystems, Inc. ATTN: R.E. Tompkins J. Kennedy 7225 Northland Dr. Brooklyn Park, MN 55428
1	AVCO Everett Research Laboratory ATTN: D. Stickler 2385 Revere Beach Parkway Everett, MA 02149-5936
1	General Applied Sciences Lab ATTN: J. Erdos 77 Raynor Ave. Ronkonkama, NY 11779-6649
1	General Electric Company Tactical System Department ATTN: J. Mandzy 100 Plastics Ave. Pittsfield, MA 01201-3698
1	IITRI ATTN: M.J. Klein 10 W. 35th Street Chicago, IL 60616-3799
5	Hercules, Inc. Radford Army Ammunition Plant ATTN: D.A. Worrell W.J. Worrell R. Goft C. Chandler L. Rivenbark Radford, VA 24141-0299
2	Hercules, Inc. Allegheny Ballistics Laboratory ATTN: William B. Walkup Thomas F. Farabaugh P.O. Box 210 Rocket Center, WV 26726
1	Hercules, Inc. Hercules Plaza ATTN: B.M. Riggleman Wilmington, DE 19894
1	MBR Research Inc. ATTN: Dr. Moshe Ben-Reuven 601 Ewing St., Suite C-22 Princeton, NJ 08540
1	Olin Corporation Badger Army Ammunition Plant ATTN: F.E. Wolf Baraboo, WI 53913
3	Olin Ordnance ATTN: E.J. Kirschke A.F. Gonzalez D.W. Worthington P.O. Box 222 St. Marks, FL 32355-0222
1	Olin Ordnance ATTN: H.A. McElroy 10101 9th Street, North St. Petersburg, FL 33716
1	Paul Gough Associates, Inc. ATTN: P.S. Gough 1048 South St. Portsmouth, NH 03801-5423
1	Physics International Library ATTN: H. Wayne Wampler P.O. Box 5010 San Leandro, CA 94577-0599
2	Princeton Combustion Research Laboratories, Inc. ATTN: N. Mer N.A. Messina Princeton Corporate Plaza 11 Deerpark Dr., Bldg IV, Suite 119 Monmouth Junction, NJ 08852

No. of Copies | Organization

3 Rockwell International
Rocketdyne Division
ATTN: BA08,
J. Flanagan
J. Gray
R.B. Edelman
6633 Canoga Avenue
Canoga Park, CA 91303-2703

2 Rockwell International Science Center
ATTN: Dr. S. Chakravarthy
Dr. S. Palaniswamy
1049 Camino Dos Rios
P.O. Box 1085
Thousand Oaks, CA 91360

1 Southwest Research Institute
ATTN: J.P. Riegel
6220 Culebra Road
P.O. Drawer 28510
San Antonio, TX 78228-0510

1 Sverdrup Technology, Inc.
ATTN: Dr. John Deur
2001 Aerospace Parkway
Brook Park, OH 44142

2 Thiokol Corporation
Elkton Division
ATTN: R. Biddle
Tech Library
P.O. Box 241
Elkton, MD 21921-0241

1 Veritay Technology, Inc.
ATTN: E. Fisher
4845 Millersport Hwy.
East Amherst, NY 14501-0305

1 Universal Propulsion Company
ATTN: H.J. McSpadden
25401 North Central Ave.
Phoenix, AZ 85027-7837

1 SRI International
Propulsion Sciences Division
ATTN: Tech Library
333 Ravenwood Avenue
Menlo Park, CA 94025-3493

No. of Copies | Organization

Aberdeen Proving Ground

1 Cdr, USACSTA
ATTN: STECS-PO/R. Hendricksen

No. of Copies	Organization
1	Ernst-Mach-Institut ATTN: Dr. R. Heiser Haupstrasse 18 Weil am Rheim Germany
1	Defence Research Agency, Military Division ATTN: C. Woodley RARDE Fort Halstead Sevenoaks, Kent, TN14 7BP England
1	School of Mechanical, Materials, and Civil Engineering ATTN: Dr. Bryan Lawton Royal Military College of Science Shrivenham, Swindon, Wiltshire, SN6 8LA England
2	Institut Saint Louis ATTN: Dr. Marc Giraud Dr. Gunther Sheets Postfach 1260 7858 Weail am Rhein 1 Germany

No. of Copies	Organization
1	Explosive Ordnance Division ATTN: A. Wildegger-Gaissmaier Defence Science and Technology Organisation P.O. Box 1750 Salisbury, South Australia 5108
1	Armaments Division ATTN: Dr. J. Lavigne Defence Research Establishment Valcartier 2459, Pie XI Blvd., North P.O. Box 8800 Courcelette, Quebec G0A 1R0 Canada
1	U.S. Army European Research Office ATTN: Dr. Roy E. Richenbach Box 65 FPO New York 09510-1500

INTENTIONALLY LEFT BLANK.

USER EVALUATION SHEET/CHANGE OF ADDRESS

This Laboratory undertakes a continuing effort to improve the quality of the reports it publishes. Your comments/answers to the items/questions below will aid us in our efforts.

1. ARL Report Number ARL-TR 80 Date of Report February 1993

2. Date Report Received _____

3. Does this report satisfy a need? (Comment on purpose, related project, or other area of interest for which the report will be used.) _____

4. Specifically, how is the report being used? (Information source, design data, procedure, source of ideas, etc.) _____

5. Has the information in this report led to any quantitative savings as far as man-hours or dollars saved, operating costs avoided, or efficiencies achieved, etc? If so, please elaborate. _____

6. General Comments. What do you think should be changed to improve future reports? (Indicate changes to organization, technical content, format, etc.) _____

CURRENT ADDRESS

_____
Organization

_____
Name

_____
Street or P.O. Box No.

_____
City, State, Zip Code

7. If indicating a Change of Address or Address Correction, please provide the Current or Correct address above and the Old or Incorrect address below.

OLD ADDRESS

_____
Organization

_____
Name

_____
Street or P.O. Box No.

_____
City, State, Zip Code

(Remove this sheet, fold as indicated, staple or tape closed, and mail.)

DEPARTMENT OF THE ARMY

OFFICIAL BUSINESS

BUSINESS REPLY MAIL
FIRST CLASS PERMIT No 0001, APG, MD

Postage will be paid by addressee

Director
U.S. Army Research Laboratory
ATTN: AMSRL-OP-CI-B (Tech Lib)
Aberdeen Proving Ground, MD 21005-5066

NO POSTAGE
NECESSARY
IF MAILED
IN THE
UNITED STATES